Title
Depolarized Scattering from Block Copolymer Grains Using Circularly Polarized Light

Journal
Macromolecules, 50(13)

ISSN
0024-9297

Authors
Wang, Xin
Li, Xiuhong
Loo, Whitney
et al.

Publication Date
2017-07-11

DOI
10.1021/acs.macromol.7b01048

Peer reviewed

Macromolecules

Article

pubs.acs.org/Macromolecules

Depolarized Scattering from Block Copolymer Grains Using Circularly Polarized Light

Xin Wang,[†] Xiuhong Li,[†] Whitney Loo,[§] Maurice C. Newstein,[‡] Nitash P. Balsara,[§,∥,⊥] and Bruce A. Garetz*[,†]

[†]Department of Chemical and Biomolecular Engineering and [‡]Department of Electrical and Computer Engineering, NYU Tandon School of Engineering, Brooklyn, New York 11201, United States

[§]Department of Chemical and Biomolecular Engineering, University of California, Berkeley, Berkeley, California 94720, United States

[∥]Environmental Energy Technologies Division and [⊥]Materials Sciences Division, Lawrence Berkeley National Laboratory, Berkeley, California 94720, United States

ABSTRACT: The grain structure of ordered block copolymer materials affects their viscoelastic, adhesive, optical, and electrical properties. Depolarized light scattering has proven to be an important method for characterizing this grain structure. In this paper, we use both theory and experiments to demonstrate the relationship between grain structure and depolarized light scattering from ordered block copolymer samples performed with crossed circular polarizers. We model the sample assuming it comprises randomly oriented ellipsoidal grains with optic axes coincident with the ellipsoid axes. We show that the scattering pattern obtained using circularly polarized (CP) light is azimuthally symmetric, in contrast to that obtained using linearly polarized (LP) light which exhibits 4-fold angular modulation. The integrated scattered power in the CP case is twice as large as that in the LP case. By simultaneously fitting CP and LP light scattering data, we obtain robust measures of parameters that characterize grain structures. In addition, CP light scattering can, in principle, be used to characterize nonrandom grain orientation distributions.

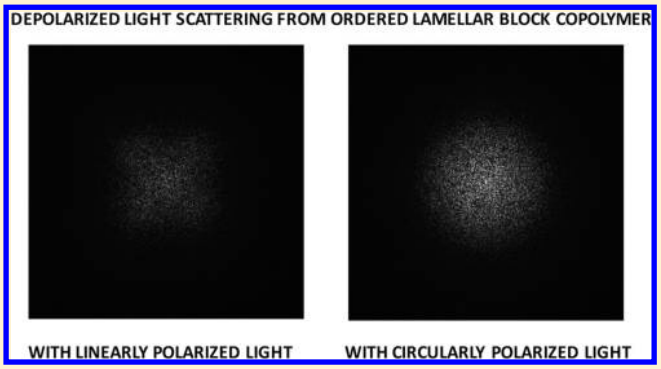

INTRODUCTION

Ordered block copolymers obtained in the absence of external fields consist of randomly oriented grains with concomitant defects. If the ordered block copolymers have lamellar or cylindrical morphology, individual grains are optically uniaxial and exhibit form birefringence, and the grain structure may be probed by depolarized light scattering (DPLS) or polarized optical microscopy (POM).[1−11] In the usual DPLS configuration, the polymer sample is illuminated with a collimated linearly polarized laser beam, and the depolarized light scattered from the sample is imaged and analyzed. In one study, experiments were conducted using circularly polarized light.[12]

The applicability of this approach for studying block copolymers was established in the 1990s. To date, it has been used not only to study order−disorder transitions and grain growth in uncharged block copolymer systems[3,5,6] but also for mixtures of block copolymers and Li^+ salts.[1,7] In addition to working out the protocols for conducting the experiments, we developed quantitative models for determining grain structure from the DPLS profiles.[2,4,13] DPLS complements conventional characterization techniques such as small-angle X-ray scattering (SAXS), small-angle neutron scattering (SANS), and electron microscopy that are geared toward determination of the geometry of local morphology (lamellae, cylinders, gyroids, etc.) on the nanometer length scale. While information about grain structure is contained in the data obtained using these methods, extracting this information is nontrivial, as demonstrated in the noteworthy work of Hashimoto et al.[14] on the estimation of grain size from SAXS and that of Stoykovich et al. and Bockstaller et al. on the use of electron microscopy for quantification of microphase connectivity and defect density.[15−23]

The grain structure of block copolymers emerges because the ordered phase forms by the process of nucleation and growth. Ordered nuclei form at random locations within the disordered phase, and grains grow at the expense of the disordered phase until they impinge on other grains, resulting in the trapping of nonequilibrium defects at grain boundaries. Grain structure is thus determined not only by the state of the system but also by its history. Depending on thermal history, one expects the emergence of grains with a variety of sizes and shapes. Obtaining robust average parameters that quantify grain structure remains challenging. In this paper, we describe how one can use both circularly and linearly polarized light to provide robust estimates of grain-structure-related parameters. In our circular-polarization scheme we illuminate the sample with left circularly polarized light and detect the right circularly polarized

Received: May 18, 2017
Revised: June 9, 2017
Published: June 26, 2017

DOI: 10.1021/acs.macromol.7b01048
Macromolecules 2017, 50, 5122−5131

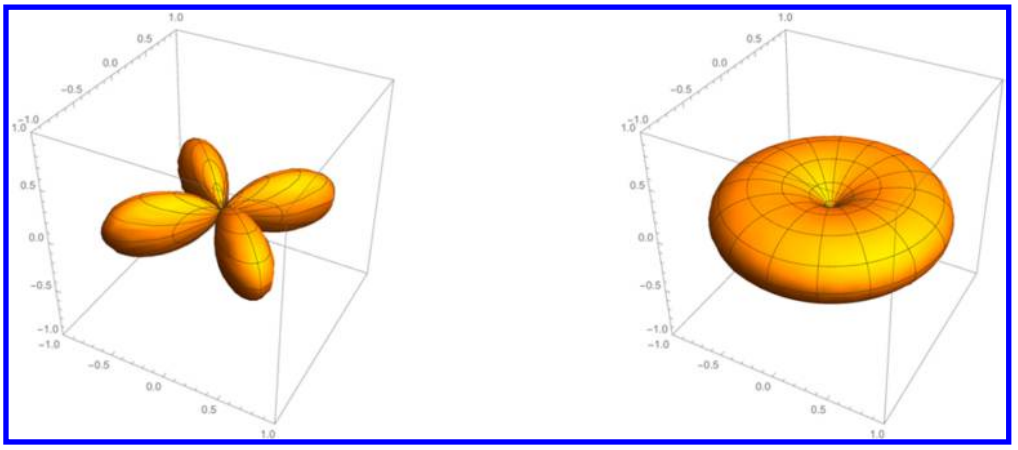

Figure 1. Polar graphs of the weighted grain orientations in depolarized light scattering with linear polarizers (left graph) and circular polarizers (right graph). The two horizontal axes are the x and y linear polarizer directions, and the vertical axis, z, is the direction of propagation of the incident light.

component of the scattered light. We show that the integrated scattered power in the circularly polarized (CP) case is twice as great as that in the linearly polarized (LP) case. While the LP patterns can exhibit 4-fold angular modulation, the CP patterns from randomly oriented grains are always azimuthally symmetric.

THEORY

A sample consisting of lamellar or cylindrical grains exhibits uniaxial form birefringence[24] with an optic axis $\vec{g}$ whose direction varies from point $\vec{r}$ to point $\vec{r}'$ in the sample. The corresponding dielectric permittivity tensor $\overleftrightarrow{\epsilon}$ can be expressed as

$$\frac{\overleftrightarrow{\epsilon}}{\epsilon_0} = n_o^2(\overleftrightarrow{I} - \vec{g}\vec{g}) + n_e^2\vec{g}\vec{g} \tag{1}$$

where $\overleftrightarrow{I}$ is the unit tensor, ϵ_0 is the vacuum permittivity, and n_e and n_o are the extraordinary and ordinary refractive indices, respectively. The term responsible for light scattering is the difference, $\delta\overleftrightarrow{\epsilon}$, between $\overleftrightarrow{\epsilon}$ and its average value, $\langle\overleftrightarrow{\epsilon}\rangle$, which can be written

$$\frac{\delta\overleftrightarrow{\epsilon}}{\epsilon_0} \simeq 2n_o(n_e - n_o)\left(\vec{g}\vec{g} - \frac{\overleftrightarrow{I}}{3}\right) \tag{2}$$

The depolarized scattered power per unit solid angle $d\Omega$ can be expressed in terms of the spatial variation of permittivity in the sample according to[25]

$$\frac{dI(\vec{q})}{d\Omega} = \frac{k^4 I_{inc}}{(4\pi)^2}\int d\vec{r}\int d\vec{r}'\frac{\langle\delta\epsilon_{12}^*(\vec{r})\delta\epsilon_{12}(\vec{r}')\rangle}{\epsilon_0^2} \times \exp[-i\vec{q}\cdot(\vec{r} - \vec{r}')] \tag{3}$$

where $\vec{q}$ is the scattering vector, k is the propagation constant, I_{inc} is the incident light intensity, $\vec{r}$ and $\vec{r}'$ are vectors representing two different locations in the sample, and $\delta\epsilon_{12}(\vec{r})$ is the tensor element of $\delta\overleftrightarrow{\epsilon}$ evaluated between orthogonal polarization states represented by complex unit vectors $\vec{a}_1$ and $\vec{a}_2$. For ideal uncorrelated ellipsoidal grains with shape axis coincident with optic axis, the averaged product of the two permittivity tensor elements can be written as

$$\frac{\langle\delta\epsilon_{12}^*(\vec{r})\delta\epsilon_{12}(\vec{r}')\rangle}{\epsilon_0^2} \simeq \left|\frac{\delta\epsilon_{12}}{\epsilon_0}\right|^2 C(\vec{R}, \vec{g}) \tag{4}$$

where $\vec{R} = \vec{r} - \vec{r}'$ and $C(\vec{R}, \vec{g})$ is an ellipsoidal correlation function given by

$$C(\vec{R}, \vec{g}) = \exp\left[-\left(\frac{\vec{g}\cdot\vec{R}}{l}\right)^2\right]\exp\left[-\frac{(\vec{l}\cdot\vec{R})^2 + (\vec{m}\cdot\vec{R})^2}{w^2}\right] \tag{5}$$

where $\{\vec{g}, \vec{l}, \vec{m}\}$ constitute an orthogonal set of unit vectors, and l and w are grain size parameters along and perpendicular to the optic axis, respectively. The assumed form of the correlation function is partly motivated by the predicted ellipsoidal shape of lamellar grains at equilibrium with a disordered phase based on the Wulff construction.[26] This yields a scattered intensity given by

$$I(\vec{q}) \propto \int_0^{2\pi}\int_0^{\pi}\sin\theta_g\, d\theta_g\, d\phi_g\, |\vec{a}_1^*\cdot\vec{g}\vec{g}\cdot\vec{a}_2|^2 \int d\vec{R}\; C(\vec{R}, \vec{g})\exp[-i(\vec{q}\cdot\vec{R})] \tag{6}$$

where θ_g and ϕ_g are the polar and azimuthal angles of $\vec{g}$, respectively. In terms of those angles, $\vec{g}$ takes the form ($\cos\phi_g \sin\theta_g$, $\sin\phi_g \sin\theta_g$, $\cos\theta_g$). In all of our previous work, we have assumed that the sample was held between linear crossed polarizers, i.e., $\vec{a}_1 = \hat{x}$ and $\vec{a}_2 = \hat{y}$. In that case, $|\vec{a}_1^*\cdot\vec{g}\vec{g}\cdot\vec{a}_2|^2$ is equal to $\frac{1}{4}\sin^4\theta_g \sin^2 2\phi_g = \frac{1}{8}\sin^4\theta_g(1 - \cos 4\phi_g)$. This leads to scattering patterns with 4-fold symmetry seen in many block copolymer samples.[4,25,27,28]

We now wish to consider the case where the sample is held between crossed circular polarizers, i.e., $\vec{a}_1 = (\hat{x} + i\hat{y})/\sqrt{2}$ and $\vec{a}_2 = (\hat{x} - i\hat{y})/\sqrt{2}$. In this case, we find that $|\vec{a}_1^*\cdot\vec{g}\vec{g}\cdot\vec{a}_2|^2$ is equal to $\frac{1}{4}\sin^4\theta_g(\sin^2 2\phi_g + \cos^2 2\phi_g) = \frac{1}{4}\sin^4\theta_g$, with no ϕ_g dependence. The absence of a ϕ_g dependence results in a scattered intensity that is azimuthally symmetric.

The term $|\vec{a}_1^*\cdot\vec{g}\vec{g}\cdot\vec{a}_2|^2$ is acting as a weighting factor in the integral in eq 6 that selectively weights the scattering contribution from each grain orientation. The two polarization schemes (linear vs circular) weight grain orientations differently. The lobes shown in the left and right graphs in Figure 1 indicate the grain orientations that preferentially contribute to the light scattering pattern for linear and circular polarization, respectively. Linear polarization weights grains whose axes are oriented 45° to the polarizer and analyzer directions, in the plane perpendicular to the direction of propagation of the

DOI: 10.1021/acs.macromol.7b01048
Macromolecules 2017, 50, 5122−5131

incident light. Circular polarization weights grains whose axes are in the plane perpendicular to the direction of propagation but independent of orientation within that plane; it thus contains contributions from twice as many grains as linear polarization, resulting in an integrated scattered power that is twice as large.

The theoretically predicted DPLS profile for the LP case, obtained from a collection of randomly oriented ellipsoidal grains with optic axis aligned with the shape axis of the ellipsoid, is gotten by integrating eq 6. In ref 27, it was shown that this results in the following expression:

$$I(q, \mu) = I_0[C_0(q; l, w) + C_4(q; l, w) \cos 4\mu] \quad (7)$$

where I_0 is the intensity in the forward direction, q is the magnitude of the scattering vector, l is the length of the major axis of the ellipsoid, w is the length of the minor axis, and μ is the azimuthal angle in the scattering plane.[27] The $C_0(q;l,w)$ component dictates the overall decay of the scattered intensity as a function of q, l, and w; the $C_4(q;l,w)$ component is a measure of the depth of the 4-fold angular modulation of the scattering patterns. In 2014, we reported the following analytic expressions for C_0 and C_4 for linear polarization.[1]

$$C_0(q; l, w) = \frac{15}{4096\alpha^{5/2}} \exp\left[-\left(\frac{qw}{2}\right)^2\right]\{-4e^{-2\alpha}\alpha^{1/2}(9 + 20\alpha) + (2\pi)^{1/2}[9 + 8\alpha(1 + 6\alpha)] \operatorname{erf}[(2\alpha)^{1/2}]\} \quad (8)$$

$$C_4(q; l, w) = -\frac{15}{4096\alpha^{5/2}} \exp\left[-\left(\frac{qw}{2}\right)^2\right]\{-20e^{-2\alpha}\alpha^{1/2}(21 + 4\alpha) + 3(2\pi)^{1/2}[35 + 8\alpha(-5 + 2\alpha)] \operatorname{erf}[(2\alpha)^{1/2}]\} \quad (9)$$

where $\alpha = \frac{(qw)^2}{8}\left[\left(\frac{l}{w}\right)^2 - 1\right]$. In the special case that grains are spherical on average ($l = w$), $C_0 = \exp[-(qw/2)^2]$ and $C_4 = 0$, and the resulting scattering pattern is azimuthally symmetric. Fitting the measured experimental DPLS data to these equations enables the determination of the characteristic length and width of the grains (l and w).[1,7,29]

Following the approach in ref 27, integrating eq 6 for the CP case yields the a much simpler expression due to the simplicity of the $|\vec{a}_1^* \cdot \vec{g}\vec{g} \cdot \vec{a}_2|^2$ term noted above.

$$I(q) = 2I_0C_0(q; l, w) \quad (10)$$

where C_0 is identical to expression from the LP case. Because $C_4 \to 0$ as $q \to 0$, eqs 7 and 10 show explicitly that the CP scattered intensity in the forward direction is predicted to be twice that found for linear polarization. Equation 10 also shows that the 4-fold modulation is absent in the CP scattering pattern. Note that the parameters I_0, l, and w in the predicted scattering profile obtained with a circularly polarized incident beam are identical to those in the profile obtained with a linearly polarized incident beam. Even though the CP scattering pattern is azimuthally symmetric, the CP pattern depends on the value of l/w, the anisotropy of the average grain shape. Thus, fitting the circular data alone to the ellipsoidal grain model yields values of l/w as well as w and I_0. We propose to improve the robustness of grain parameters obtained by DPLS by simultaneously fitting the linear and circular data. During data collection, we can switch between linear and circular polarization by translating a pair of quarter wave plates into and out of the light path.

One can generalize the results above to two orthogonal elliptical polarizations, $\vec{a}_1 = (\hat{x} + e^{i\Phi}\hat{y})/\sqrt{2}$ and $\vec{a}_2 = (-e^{-i\Phi}\hat{x} + \hat{y})/\sqrt{2}$, where Φ is a phase angle between 0 and 2π. Special cases include left and right circular polarization ($\Phi = \pi/2, 3\pi/2$) and $\pm 45°$ linear polarization ($\Phi = 0, \pi$). The resulting scattered intensity becomes

$$I(q, \mu) = I_0[(1 + \sin^2\Phi)C_0(q; l, w) - (1 - \sin^2\Phi) \times C_4(q; l, w) \cos 4\mu] \quad (11)$$

As Φ increases from 0 to $\pi/2$, the pattern changes continuously from the LP pattern to the CP pattern, so there is no new information to be gained from the use of elliptical polarization. The minus sign in front of the C_4 term arises because the incident linear polarization is rotated 45° relative to the incident $\hat{x}$ polarization used in the earlier derivation.

In a simplified "slab" model published in 1992, we derived an expression for the total power, P, exiting a block copolymer sample held between perfectly crossed linear polarizers, assuming that incident light propagates without diffraction through a series of randomly oriented grains, each exhibiting a very weak birefringence.[30] This is obtained in the limit where the average lateral grain size is much larger than the wavelength of light, so that all of the scattered rays essentially point along the direction of propagation. The cumulative effect of light propagating through these grains was calculated using Jones calculus according to the equation

$$\vec{V}_{out} = [\Pi_j \vec{\vec{M}}_j]\vec{V}_{in} \quad (12)$$

where $\vec{V}_{in}$ and $\vec{V}_{out}$ are complex two-component vectors representing the input and output polarization states, respectively, and $\vec{\vec{M}}_j$ is the 2×2 Jones matrix that represents the transformation in polarization state induced by the jth grain:

$$\vec{\vec{M}}_j(\theta_j, \phi_j, l_j) = \begin{pmatrix} \cos\frac{\Gamma_j}{2} - i\cos 2\phi_j \sin\frac{\Gamma_j}{2} & -i\sin 2\phi_j \sin\frac{\Gamma_j}{2} \\ -i\sin 2\phi_j \sin\frac{\Gamma_j}{2} & \cos\frac{\Gamma_j}{2} + i\cos 2\phi_j \sin\frac{\Gamma_j}{2} \end{pmatrix} \quad (13)$$

$\Gamma_j(\theta_j, l_j) \simeq \frac{2\pi l_j}{\lambda}\Delta n \sin^2\theta_j$ is the phase shift due to the jth grain, θ_j and ϕ_j are the polar and azimuthal angles that the jth grain optic axis makes with respect to the direction of propagation, z, $\Delta n = (n_e - n_o)$, l_j is the length of the grain in the z-direction, and λ is the wavelength of the incident light. If the incident light is x-polarized, $\vec{V}_{in} = \begin{pmatrix} 1 \\ 0 \end{pmatrix}$, and to first order in Γ_j,

$$\vec{V}_{out} \simeq \begin{pmatrix} 1 - \Sigma_j \frac{i\Gamma_j}{2}\cos 2\phi_j \\ -\Sigma_j \frac{i\Gamma_j}{2}\sin 2\phi_j \end{pmatrix} \quad (14)$$

The power of light transmitted through a y-polarizer is given by

$$\left(\frac{P}{P_0}\right)_{LP} = \left|\begin{pmatrix} 0 & 0 \\ 0 & 1 \end{pmatrix}\vec{V}_{out}\right|^2 = \left(\frac{\pi\Delta n}{\lambda}\right)^2 \Sigma_j l_j^2 \sin^4\theta_j \sin^2 2\phi_j = \left(\frac{\pi\Delta n}{\lambda}\right)^2 N\langle l^2\rangle\langle\sin^4\theta\rangle\langle\sin^2 2\phi\rangle = \frac{4\pi^2}{15}(\Delta n)^2 N\frac{\langle l^2\rangle}{\lambda^2} \quad (15)$$

DOI: 10.1021/acs.macromol.7b01048
Macromolecules 2017, 50, 5122−5131

where $\langle\ \rangle$ indicates average values, P_0 is the incident power, and N is the total number of grains. We have assumed that the sum of cross terms involving two different grains in eq 15 equals zero because the grains are uncorrelated. In terms of the sample path length $L = N\langle l\rangle$, the transmitted power becomes

$$\left(\frac{P}{P_0}\right)_{LP} = \frac{4\pi^2}{15}(\Delta n)^2\frac{Ll_{av}}{\lambda^2} \tag{16}$$

where $l_{av} \equiv \langle l\rangle^2/\langle l\rangle$ is the average grain size.

If the incident light is left circularly polarized, $\vec{V}_{in} = \frac{1}{\sqrt{2}}\begin{pmatrix}1\\ i\end{pmatrix}$, and

$$\vec{V}_{out} \simeq \frac{1}{\sqrt{2}}\begin{pmatrix} 1 - \Sigma_j\frac{i\Gamma_j}{2}\cos 2\phi_j + \Sigma_j\frac{i\Gamma_j}{2}\sin 2\phi_j \\ i\left(1 + \Sigma_j\frac{i\Gamma_j}{2}\cos 2\phi_j - \Sigma_j\frac{i\Gamma_j}{2}\sin 2\phi_j\right)\end{pmatrix} \tag{17}$$

The power transmitted through a right-circular polarizer is given by

$$\left(\frac{P}{P_0}\right)_{CP} = \left|\frac{1}{2}\begin{pmatrix}1 & i\\ -i & 1\end{pmatrix}\vec{V}_{out}\right|^2 = \left(\frac{\pi\Delta n}{\lambda}\right)^2 N\langle l^2\rangle\langle\sin^4\theta\rangle$$
$$\times\left(\langle\sin^2 2\phi\rangle + \langle\cos^2 2\phi\rangle\right) = \left(\frac{\pi\Delta n}{\lambda}\right)^2 N\langle l^2\rangle\langle\sin^4\theta\rangle$$
$$= \frac{8}{15}(\Delta n)^2 N\frac{\langle l^2\rangle}{\lambda^2} \tag{18}$$

which can be re-expressed as

$$\left(\frac{P}{P_0}\right)_{CP} = \frac{8\pi^2}{15}(\Delta n)^2\frac{Ll_{av}}{\lambda^2} \tag{19}$$

The resulting CP transmitted power is exactly double the LP transmitted power. Note that the θ and ϕ dependences in eqs 15 and 18 are identical to the θ and ϕ dependences in the weighting factors in eq 6. The total transmitted power can also be calculated for the ellipsoidal grain model by integrating eqs 7 or 10 over all values of q and μ. In eq 7, the cos 4 μ term integrates to zero, leaving only the integral of $I_0C_0(q)$, and in eq 10, we have the integral of $2I_0C_0(q)$, yielding an integrated CP power exactly twice the integrated LP power, consistent with the results of the "slab" model.

EXPERIMENTAL SECTION

Materials and Sample Preparation. A polystyrene-*b*-poly(ethylene oxide), SEO, diblock copolymer was synthesized, purified, and characterized as outlined in ref 31. The diblock copolymer used in this study is referred to as SEO(6.4−7.3), where 6.4 and 7.3 are the number-averaged molecular weights of the polystyrene (PS) and poly(ethylene oxide) (PEO) blocks in kg mol^{-1}, respectively. The polydispersity index of the diblock copolymer is 1.04.

The sample used in the DPLS experiments was made in Berkeley. First the freeze-dried block copolymer was melted into a 1/32 in. thick annular Viton rubber spacer (McMaster Carr) with an inner diameter of 3/16 in. at 120 °C until a transparent, bubble-free sample was obtained. Then the sample was placed between two quartz windows in a custom-built airtight aluminum sample holder. The sample was vacuum-sealed in an aluminum-reinforced polypropylene pouch in an argon glovebox for delivery to Brooklyn for the DPLS measurement. When quiescently ordered, such millimeter-thick samples consist of randomly oriented grains, unlike sub-micrometer-thick samples, which exhibit preferential alignment of lamellae or cylinders with respect to the sample−substrate interface.[32]

Small-Angle X-ray Scattering. Small-angle X-ray scattering (SAXS) measurements were performed to confirm the T_{ODT}. SAXS samples were prepared by pressing/melting the polymer into 1/32 in. thick annular Viton rubber spacers (McMaster Carr) with an inner diameter of 1/8 in. at 120 °C and annealing them at 120 °C for at least 12 h. The samples were sealed with Kapton windows in custom-designed airtight holders. The samples were mounted in a custom-built 8-sample stage and annealed at each temperature for 30 min before taking measurements.

SAXS measurements were conducted at beamline 1-5 at the Stanford Synchrotron Radiation Lightsource (SSRL) at SLAC National Accelerator Laboratory. Silver behenate was used to determine the beam center and sample-to-detector distance. The scattered intensity was corrected for beam transmission, empty cell scattering, as well as for unavoidable air gaps in the system. Two-dimensional scattering patterns were integrated azimuthally using the Nika program for Igor Pro to produce one-dimensional scattering profiles, shown in Figure 2.[33] The T_{ODT} was determined by finding the discontinuity in the full width at half-maximum (fwhm) of the scattering peaks with respect to temperature. In Figure 3, one observes the discontinuity at a temperature between 76 and 81 °C. We conclude that the order-to-disorder transition temperature, T_{ODT}, of the material is 78 ± 2 °C. Below the T_{ODT}, the diblock copolymer forms an ordered phase with a lamellar microstructure, as determined by SAXS analysis.

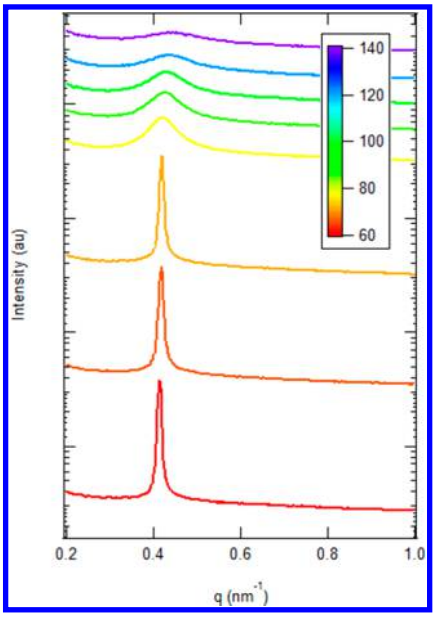

Figure 2. One-dimensional SAXS profiles as a function of temperature, showing the broadening of the primary lamellar scattering peak with increasing temperature.

The polymer used in this study was obtained by purifying an SEO polymer using a neutral alumina column, as described in ref 34. We found that the composition of the purified polymer differed measurably from that of the original, as synthesized, copolymer. Although we were unable to detect any difference between different batches of purified polymer by either NMR or gel permeation chromatography, the measured T_{ODT} value varied from batch to batch. Another batch of SEO(6.4-7.3) used in ref 31 exhibited a T_{ODT} value of 107.5 °C. We posit that PEO-rich copolymer chains are retained in the alumina column to different extents, depending on the details such as polymer concentration, column history, etc. Further work is needed to ensure batch-to-batch consistency in our SEO samples. The uncertainty in T_{ODT} does not affect any of the conclusions in this paper.

DPLS Measurement. A custom-made apparatus was used for performing the light scattering experiments; a schematic is shown in Figure 4.

DOI: 10.1021/acs.macromol.7b01048
Macromolecules 2017, 50, 5122−5131

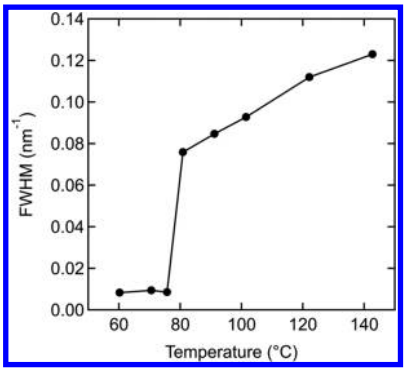

Figure 3. Plot of SAXS scattering peak full width at half-maximum as a function of temperature, showing discontinuity associated with the order−disorder transition at 78 ± 2 °C.

It is similar to the apparatus described in ref 2 except for the addition of two quarter-wave retardation plates. A Coherent continuous-wave diode laser with wavelength of 640 nm and an output power adjustable from 0 to 40 mW was the light source for the apparatus.

By rotating the half-wave plate placed between the laser and the polarizer, the intensity of the light incident on the sample could be adjusted. We chose to use 5 mW to avoid saturating the CCD camera. In the traditional configuration, the sample was illuminated with linearly polarized light created by the first polarizer, and orthogonally polarized scattered light generated in the sample was selected using the second crossed polarizer. In the new configuration, two quarter-wave plates were added: one after the polarizer with its fast axis at +45° to the polarizer axis and the other before the analyzer with its fast axis at −45° to the polarizer axis.

The first quarter-wave plate converted the incident linear polarization to circular polarization, and the second quarter-wave plate converted the orthogonal circularly polarized component of the scattered light generated by the sample into linear polarization that was completely transmitted by the analyzer. The scattered light that passed through the analyzer formed a scattering pattern on an Edmundoptics ground glass screen that was recorded by a Lumenera CCD camera (INFINITY2-1R) controlled by a custom-programmed interface. The two quarter-wave plates were mounted on a single optical rail and could be translated into and out of the optical path without requiring any additional alignment to quickly switch between linear and circular DPLS measurements.

The temperature of the heating block was varied using two heating elements connected to an Omega Engineering temperature controller (CN9111A). The relationship between the controller temperature and the actual sample temperature was established by a separate experiment described in ref 1. Before conducting the depolarized light scattering experiments, the sample was first heated to 110 °C in the heating block to erase any thermal processing history. After 1 h, the temperature controller was set to 68 °C which constituted the start of the quenching process. At the same time, the first two scattering patterns were recorded, one with and one without the quarter-wave plates in the beam path, and they were used as background noise patterns that were subtracted from subsequently recorded CP and LP scattering patterns, respectively. Five hours later, two more scattering patterns were captured, one with and one without quarter-wave plates in the beam path. All of the scattering patterns were stored in the form of 8-bit, 801 × 801 pixel TIFF image files. The intensity at each pixel was recorded as a dimensionless number between 0 and 255. The resulting LP and CP scattering patterns are shown in Figure 5.

DPLS Data Reduction and Analysis. As seen in Figure 5, the scattering patterns exhibit a speckle pattern, which is due to the interference of scattered light from different grains in the sample. The high-spatial-frequency components of the speckle were eliminated by low-pass filtering, in which the image is convoluted with a Gaussian function with a fwhm of 12 pixels.

In order to estimate values of l, w, and I_0, three cosine moments $f_0(q)$, $f_4(q)$, and $g_0(q)$ were extracted from the experimentally measured linear and circular scattering patterns, I_{LP} and I_{CP}, and were least-squares fitted to C_0 and C_4 according to

$$f_0(q) = \int_0^{2\pi} I_{LP}(q, \mu)\, d\mu = 2\pi I_0 C_0(q; l, w) \tag{20}$$

$$f_4(q) = \int_0^{2\pi} I_{LP}(q, \mu) \cos 4\mu\, d\mu = \pi I_0 C_4(q; l, w) \tag{21}$$

$$g_0(q) = \int_0^{2\pi} I_{CP}(q, \mu)\, d\mu = 4\pi I_0 C_0(q; l, w) \tag{22}$$

We also extracted a fourth cosine moment, $g_4(q)$, which is exactly zero for all q according to the ellipsoidal grain model:

$$g_4(q) = \int_0^{2\pi} I_{CP}(q, \mu) \cos 4\mu\, d\mu = 0 \tag{23}$$

Each cosine moment was numerically integrated for 136 values of q between 0 and 1.4 μm^{-1}. A subset of those values is plotted using symbols in Figure 6.

The Levenberg−Marquardt method was used for the nonlinear least-squares fitting of the cosine moments to the single ellipsoidal grain model.[35] Figure 6 shows the results of the least-squares fitting of all three cosine moments (dashed lines). The fits to the moments $f_0(q)$ and $g_0(q)$ are excellent, while the fit to $f_4(q)$ is relatively poor, although one should note that $f_4(q)$ is enhanced by a factor of 10 in Figure 6 to highlight this mismatch. The poor fit of $f_4(q)$ has often been observed in our earlier experimental studies.[1,7,36] What is remarkable is that the fits are so good given the substantial and varied

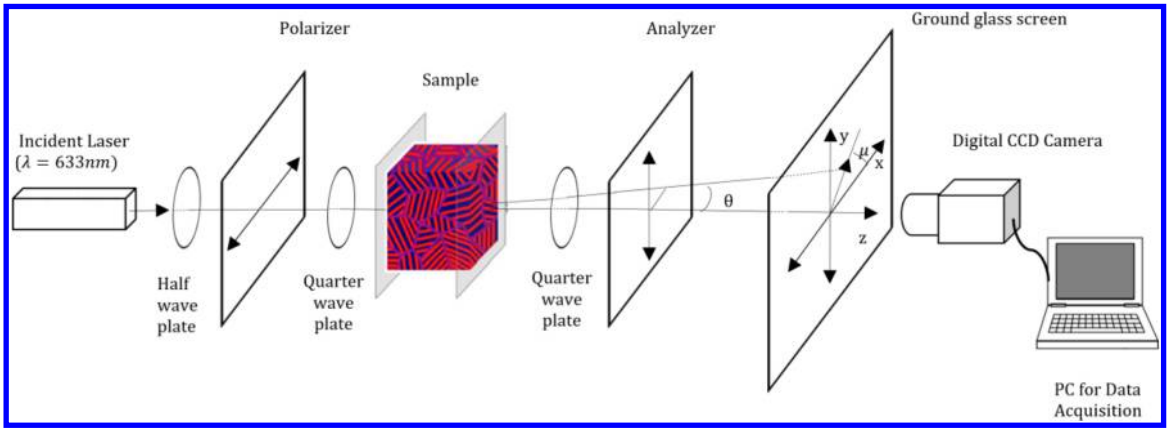

Figure 4. Schematic of the DPLS apparatus for determining grain structure. The apparatus was used to probe the sample using either linearly (by removing the quarter-wave plates) or circularly polarized beams (as shown).

DOI: 10.1021/acs.macromol.7b01048
Macromolecules 2017, 50, 5122−5131

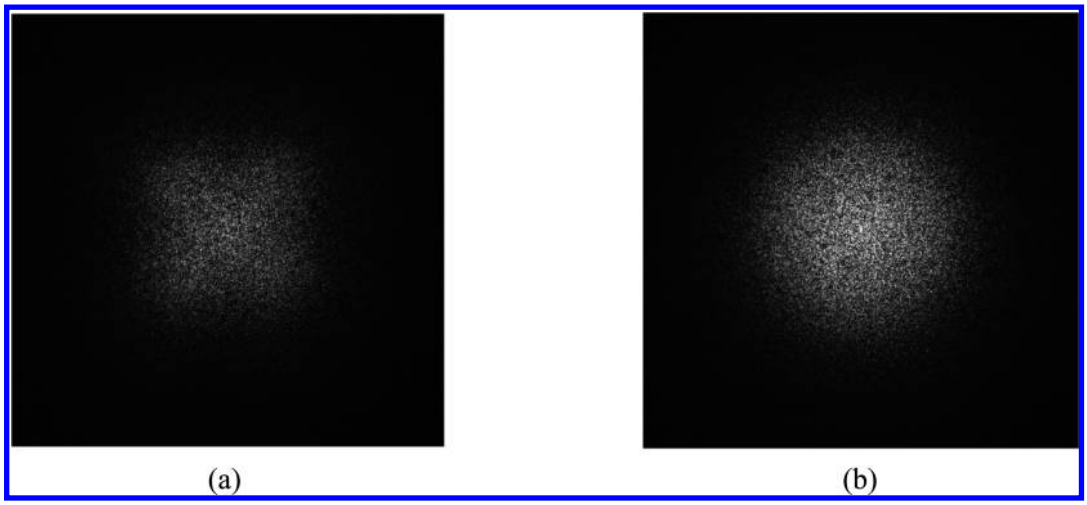

Figure 5. Parts a and b represent LP and CP scattering patterns, respectively. The quench depth was 15 °C. The maximum scattering vector q at the sides of each image is 1.48 μm^{-1}. The contrast of the two patterns has been identically adjusted to enhance major features that were not clear in the original low-intensity patterns.

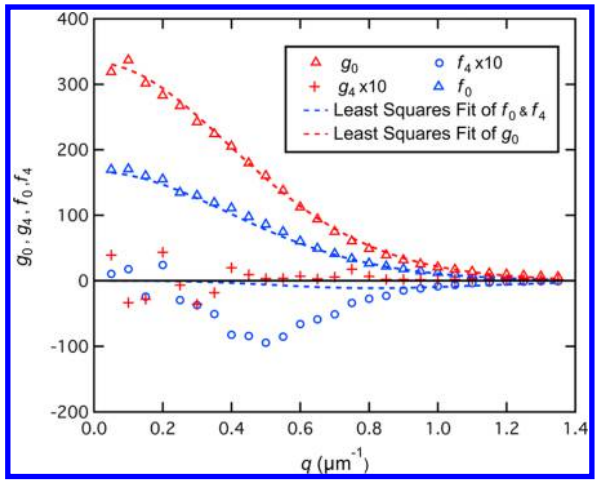

Figure 6. Least-squares fit of experimentally extracted $f_0(q)$, $f_4(q)$, and $g_0(q)$ functions from the scattering patterns in Figure 5. The grain parameters obtained from this fit are l/w = 1.79, w = 2.63 μm, and I_0 = 27.6.

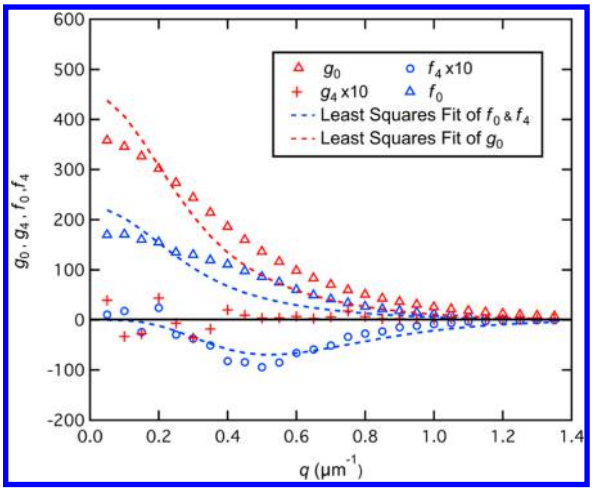

Figure 7. Least-squares fit of experimentally extracted $f_0(q)$, $f_4(q)$, and $g_0(q)$ functions from the scattering patterns in Figure 5, but minimizing the fractional error rather than the absolute error. The grain parameters obtained from this fit are l/w = 3.54, w = 2.64 μm, and I_0 = 35.8.

complexities of block copolymer grain defect structure and that the model has only three parameters to fit all three cosine moments. The moment $g_4(q)$ is close to zero as expected from eq 23. It is possible to obtain a better fit to $f_4(q)$ by weighting the cosine moments differently during the least-squares fitting. For example, one can minimize the sum of the squares of the *fractional* error rather than the *absolute* error. Figure 7 shows such a fit, in which we minimize the sum of the squares of the errors divided by the sum of squares of the values for each cosine moment. One sees a much better fit to $f_4(q)$ but at the expense of extremely poor fits to $f_0(q)$ and $g_0(q)$. Since $f_0(q)$ and $g_0(q)$ determine the overall size of the scattering pattern, while $f_4(q)$ describes mainly the 4-fold modulation, it is much more important to fit them well rather than $f_4(q)$ We conclude that minimizing the absolute error is a superior approach to obtaining accurate grain parameters.

According to eqs 20 and 22, the ratio $g_0(q)/f_0(q)$ should be exactly 2 for all values of q. This ratio is plotted in Figure 8. As seen in this figure, the experimentally obtained ratio is close to 2 at small q but appears to have a systematic falloff for larger q values. We believe that this falloff is due to very weak stray background light reaching the ground glass screen that is not totally eliminated by subtracting background noise patterns. For simplicity, this weak background is assumed to be uniform across the screen, in which case its effect on moments $f_0(q)$ and $g_0(q)$ is a constant offset, independent of q. Within the ellipsoidal grain model, this ratio therefore would have the form

$$\left(\frac{g_0(q)}{f_0(q)}\right)_{\text{model+stray}} = \frac{4\pi I_0 C_0(q) + b}{2\pi I_0 C_0(q) + b} \leq 2 \tag{24}$$

where b is a constant. The dotted line shown in Figure 8 is a least-squares fit to this expression, with b taking on the value of 2.6. This value of b corresponds to each pixel having 2.6 extra units of intensity on average (out of a maximum 255) due to stray light. The fit is within experimental error for most values of q.

In an effort to understand the relative merits of fitting different combinations of cosine moments, we carried out three separate least-squares fits: using the LP data alone (f_0, f_4), the CP data alone (g_0), and the LP and CP data in combination (f_0, f_4, g_0). A least-squares fitting involves the minimization of χ^2, the sum of the squares of the differences between the values of the experimental cosine moments, and the values of the theoretical functions given on the right-hand sides of eqs 20–22, as the values of the three parameters (w, l/w, I_0) are varied. If χ^2 exhibits a high curvature near the minimum, then the value of the parameter is well determined. Figure 9 shows plots of

DOI: 10.1021/acs.macromol.7b01048
Macromolecules 2017, 50, 5122–5131

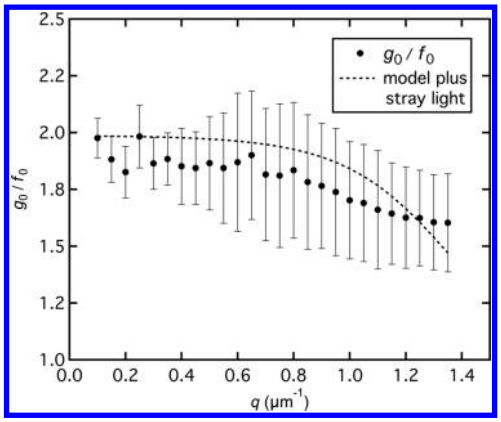

Figure 8. Ratio $g_0(q)/f_0(q)$ as a function of q extracted from the scattering patterns shown in Figure 5. The ratio is close to the theoretically predicted value of 2. Dotted line is a fit to the ellipsoidal grain model, including the effect of stray light reaching the detection screen.

three projections of χ^2 in the vicinity of the minimum. For each projection, we plot χ^2 as a function of one parameter, with the other two parameters held fixed with their minimized values. Also for each projection, we plot χ^2 for the LP, CP, and LP+CP fits. One observes two features of these plots. First, the positions of the minima are slightly different depending of which data set one chooses. Second, and more importantly, the curvature at the minimum is greatest when one fits linear and circular data together (blue curves). In other words, the simultaneous fitting of the linear and circular data provides the most robust determination of all three parameters. Table 1 shows the best-fit parameters for the three fits.

Sometimes one encounters an ordered block copolymer sample with a background global birefringence.[36] Such a birefringence complicates the DPLS measurement because it allows a portion of the incident beam to leak through the crossed polarizers, generating a bright central spot in the center of the scattering pattern. With the usual linear DPLS, it can be eliminated by rotating the sample until the optic axis of the global birefringence is coincident with the polarizer axis.

This method would not work for circular DPLS, since there is no polarization axis. In that case, however, it could be eliminated using a Soliel-Babinet compensator placed before or after the sample, as was done in ref 12.

CONCLUSIONS

In summary, we have explored the relationship between the depolarized light scattering signal from an ordered block copolymer sample and grain structure for both linearly and circularly polarized light. The integrated scattered power for circularly polarized light is twice that for linearly polarized light. While the linearly polarized case yields scattering patterns with 4-fold angular modulation for a random collection of ellipsoidal grains, the circularly polarized case yields scattering patterns that are azimuthally symmetric. We show that the grain parameters determined by the simultaneous fitting of linear and circular light scattering data provides a more robust determination of the three ellipsoidal grain model parameters, l, w, and I_0 than those obtained by fitting the linear and circular scattering data separately. This represents an important improvement to the technique of DPLS for the characterization of the grain structure in block copolymer materials.

Block copolymers are characterized by structures on two length scales: local morphology (e.g., lamellae) on the molecular length scale (typically 10 nm) and grain structure (typically 1−10 μm). While characterization techniques to quantify structure

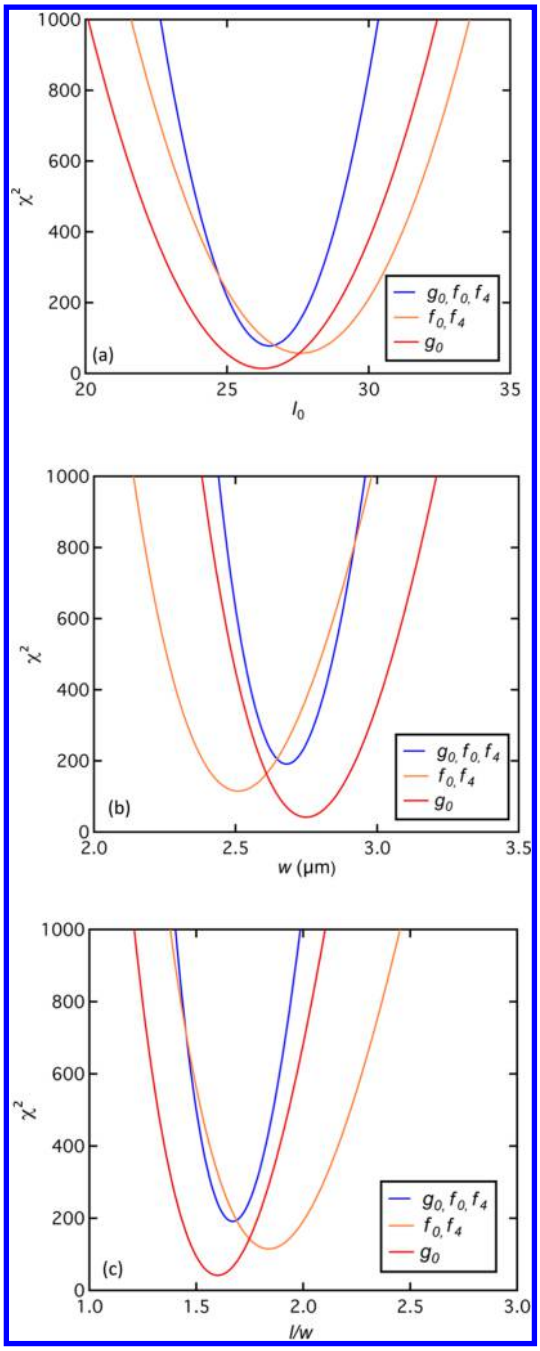

Figure 9. Projections of $\chi^2\left(I_0, w, \frac{l}{w}\right)$ in the vicinity of the least-squares minimum. Parts a, b, and c represent χ^2 as a function of I_0, w, and $\frac{l}{w}$, respectively. In each part, the red, yellow, and blue curves represent fits of CP data, LP data, and CP+LP data, respectively.

Table 1. Best-Fit Grain Parameters for Three Different Least-Squares Fitting Schemes

parameter	LP+CP	LP	CP
I_0	27.6 ± 0.2	28.9 ± 0.3	27.2 ± 0.3
w (μm)	2.63 ± 0.09	2.41 ± 0.10	2.72 ± 0.16
l/w	1.79 ± 0.11	2.07 ± 0.15	1.70 ± 0.18

on the molecular length scale in both position and reciprocal space are well-established, the quantification of grain structure is less well established. The dispersity of grain parameters

DOI: 10.1021/acs.macromol.7b01048
Macromolecules 2017, 50, 5122−5131

necessitates the development of statistical models, and while there has been some progress on establishing relationships between parameters determined in position and reciprocal space, much work remains to be done.[4] The present paper demonstrates that depolarized scattering using both linearly and circularly polarized light is a powerful technique for determining grain structure in reciprocal space. Our work thus far is limited to randomly oriented grains obtained by quiescently quenching a disordered block copolymer. The present technique can, in principle, be extended to analyze the grain structure from samples with macroscopically aligned grains. A random grain orientation distribution function has the form $\sin\theta_g$ as seen in eq 6. An azimuthally anisotropic distribution of ellipsoidal grains can be expressed by the function $f(\phi_g)\sin\theta_g$, where $f(\phi_g)$ can be expanded in a Fourier series in ϕ_g: $f(\phi_g) = 1 + \sum_{m=1}^{\infty}(a_{2m}\cos 2m\phi_g + b_{2m}\sin 2m\phi_g)$. In the same way that the 4-fold modulation of $|\vec{a}_1^*\cdot\vec{g}\vec{g}\cdot\vec{a}_2|^2$ for LP light leads to the 4-fold angular modulation of the LP scattered intensity, any $2m$-fold angular modulation in the grain orientation distribution is reflected in a corresponding $2m$-fold angular modulation in the intensity of the CP scattering pattern. Thus, the measurement of angular modulations in CP depolarized scattering patterns can potentially be used to characterize anisotropies in grain orientation distributions. While it has long been recognized that practically important properties of block copolymer systems such as shear modulus and ionic conductivity are related to both local morphology and grain structure, predictive relationships have not yet been established.[37−41] The present paper is but one step toward establishing such relationships.

AUTHOR INFORMATION

Corresponding Author

*(B.A.G.) E-mail: bgaretz@nyu.edu.

ORCID

Nitash P. Balsara: 0000-0002-0106-5565

Bruce A. Garetz: 0000-0002-3141-7840

Notes

The authors declare no competing financial interest.

ACKNOWLEDGMENTS

Primary funding for this work was provided by the National Science Foundation through Awards DMR-1505444 and DMR-1505476. Any opinions, findings and conclusions or recommendations expressed in this paper are those of the authors and do not necessarily reflect the views of the National Science Foundation. SAXS experiments were conducted at the Stanford Synchrotron Radiation Lightsource, a user facility at SLAC National Accelerator Laboratory supported by the U.S. Department of Energy, Office of Science, Office of Basic Energy Sciences, under Contract DE-AC02-76SF00515.

NOMENCLATURE

Abbreviations

CCD	charge coupled device
CP	circularly polarized
DPLS	depolarized light scattering
fwhm	full width at half-maximum
LP	linearly polarized
ODT	order-to-disorder transition
PEO	poly(ethylene oxide)
POM	polarized optical microscopy
PS	polystyrene
SANS	small-angle neutron scattering
SAXS	small-angle X-ray scattering
SEO	polystyrene-*b*-poly(ethylene oxide)
TIFF	tagged image file format

Symbols

$\vec{a}_1$	complex unit vector for incident polarization state, dimensionless
$\vec{a}_2$	complex unit vector for scattered polarization state, dimensionless
b	constant for stray light correction to cosine moments, dimensionless
$C(\vec{R},\vec{g})$	ellipsoidal correlation function, dimensionless
$C_0(q;l,w)$	azimuthally symmetric component of theoretical scattering intensity, dimensionless
$C_4(q;l,w)$	4-fold modulated component of theoretical scattering intensity, dimensionless
$f_0(q)$	zeroth cosine moment of experimental LP scattered intensity, dimensionless
$f_4(q)$	fourth cosine moment of experimental LP scattered intensity, dimensionless
$g_0(q)$	zeroth cosine moment of experimental CP scattered intensity, dimensionless
$\vec{g}$	unit vector in direction of grain optic axis, dimensionless
$\vec{\vec{I}}$	unit tensor, dimensionless
I_{inc}	incident light intensity, W/m^2
I_0	scattered depolarized intensity in forward direction with LP light, dimensionless
$I(q,\mu)$	scattered depolarized intensity as a function of q and μ, dimensionless
k	propagation constant of incident light, μm^{-1}
l	characteristic grain length in ellipsoidal grain model, μm
l_{av}	average grain length in "slab" model, μm
l_j	thickness of jth grain in slab model, μm
$\vec{l}$	unit vector perpendicular to both $\vec{g}$ and $\vec{m}$, dimensionless
L	sample thickness in "slab" model, μm
$\vec{m}$	unit vector perpendicular to both $\vec{g}$ and $\vec{l}$, dimensionless
$\vec{\vec{M}}_j$	Jones matrix associated with jth grain in slab model, dimensionless
n_e	extraordinary refractive index of a grain, dimensionless
n_o	ordinary refractive index of a grain, dimensionless
P	total power transmitted through sample between crossed polarizers, W
P_0	power incident on sample, W
$\vec{q}$	scattering vector, μm^{-1}
q	magnitude of scattering vector, μm^{-1}
$\vec{r}$	position vector representing a location in a sample, μm
$\vec{r}'$	position vector representing a different location in a sample, μm
$\vec{R}$	vector representing difference between two position vectors, $\vec{r}-\vec{r}'$, μm
$\vec{V}_{in}$	Jones vector representing incident light polarization in slab model, dimensionless
$\vec{V}_{out}$	Jones vector representing output light polarization in slab model, dimensionless
w	characteristic grain width in ellipsoidal grain model, μm
$\hat{x}$	unit vector representing x-polarized light, dimensionless

DOI: 10.1021/acs.macromol.7b01048
Macromolecules 2017, 50, 5122−5131

$\hat{y}$ unit vector representing y-polarized light, dimensionless

Greek Letters

α parameter in ellipsoidal grain model, a function of q, w and l/w, dimensionless
$\delta\vec{\epsilon}$ difference between local permittivity tensor and its average value, F/m
$\delta\epsilon_{12}$ tensor element of the permittivity difference tensor, $\delta\vec{\epsilon}$, F/m
Δn difference between ordinary and extraordinary refractive index, dimensionless
$\vec{\epsilon}$ permittivity tensor, F/m
$\langle\vec{\epsilon}\rangle$ average of permittivity tensor, F/m
ϵ_0 permittivity of the vacuum, F/m
Γ_j phase shift due to jth grain in slab model, dimensionless
θ_g polar angle of $\vec{g}$, rad
θ_j polar angle of jth grain in slab model, rad
λ wavelength of incident light, nm
μ azimuthal scattering angle, rad
χ^2 least-squares of experimental and theoretical scattered intensity, dimensionless
ϕ_g azimuthal angle of $\vec{g}$, rad
ϕ_j azimuthal angle of jth grain in slab model, rad
Φ phase angle in defining elliptical polarization states, rad
Ω solid angle, sr

REFERENCES

(1) Wang, X.; Thelen, J. L.; Teran, A. A.; Chintapalli, M.; Nakamura, I.; Wang, Z. G.; Newstein, M. C.; Balsara, N. P.; Garetz, B. A. Evolution of Grain Structure during Disorder-to-Order Transitions in a Block Copolymer/Salt Mixture Studied by Depolarized Light Scattering. *Macromolecules* **2014**, *47* (16), 5784−5792.

(2) Newstein, M. C.; Garetz, B. A.; Dai, H. J.; Balsara, N. P. Light-Scattering and Microscopy from Block-Copolymers with Cylindrical Morphology. *Macromolecules* **1995**, *28* (13), 4587−4597.

(3) Kim, W. G.; Chang, M. Y.; Garetz, B. A.; Newstein, M. C.; Balsara, N. P.; Lee, J. H.; Hahn, H.; Patel, S. S. Effect of quench depth on grain structure in quiescently ordered block copolymers. *J. Chem. Phys.* **2001**, *114* (22), 10196−10211.

(4) Chang, M. Y.; Abuzaina, F. M.; Kim, W. G.; Gupton, J. P.; Garetz, B. A.; Newstein, M. C.; Balsara, N. P.; Yang, L.; Gido, S. P.; Cohen, R. E.; Boontongkong, Y.; Bellare, A. Analysis of grain structure in partially ordered block copolymers by depolarized light scattering and transmission electron microscopy. *Macromolecules* **2002**, *35* (11), 4437−4447.

(5) Balsara, N. P.; Perahia, D.; Safinya, C. R.; Tirrell, M.; Lodge, T. P. Birefringence Detection of the Order-to-Disorder Transition in Block Copolymer Liquids. *Macromolecules* **1992**, *25* (15), 3896−3901.

(6) Stepanek, P.; Almdal, K.; Lodge, T. P. Polarized and depolarized dynamic light scattering from a block copolymer melt. *J. Polym. Sci., Part B: Polym. Phys.* **1997**, *35* (10), 1643−1648.

(7) Wang, X.; Chintapalli, M.; Newstein, M. C.; Balsara, N. P.; Garetz, B. A. Characterization of a Block Copolymer with a Wide Distribution of Grain Sizes. *Macromolecules* **2016**, *49* (21), 8198−8208.

(8) Chastek, T. Q.; Lodge, T. P. Measurement of gyroid single grain growth rates in block copolymer solutions. *Macromolecules* **2003**, *36* (20), 7672−7680.

(9) Chastek, T. Q.; Lodge, T. P. Grain shapes and growth kinetics of the cylinder phase in a block copolymer solution. *Macromolecules* **2004**, *37* (13), 4891−4899.

(10) Lam, C. N.; Olsen, B. D. Phase transitions in concentrated solution self-assembly of globular protein-polymer block copolymers. *Soft Matter* **2013**, *9* (8), 2393−2402.

(11) Lee, D. H.; Lee, H.; Lee, Y.; Kim, Y.; Ryu, D. Y. Enthalpic and Volumetric Changes at Phase Transitions of Polystyrene-b-poly(alkyl methacrylate) Copolymers and Their Pressure Dependence. *Macromolecules* **2014**, *47* (6), 2169−2173.

(12) Amundson, K.; Helfand, E.; Patel, S. S.; Quan, X.; Smith, S. D. Optical Characterization of Ordering and Disordering of Block Copolymer Microstructure. *Macromolecules* **1992**, *25* (7), 1935−1940.

(13) Garetz, B. A.; Newstein, M. C.; Dai, H. J.; Jonnalagadda, S. V.; Balsara, N. P. Birefringence and Diffraction of Light in Ordered Block-Copolymer Materials. *Macromolecules* **1993**, *26* (12), 3151−3155.

(14) Shibayama, M.; Hashimoto, T. Small-Angle X-Ray-Scattering Analyses of Lamellar Microdomains Based on a Model of One-Dimensional Paracrystal with Uniaxial Orientation. *Macromolecules* **1986**, *19* (3), 740−749.

(15) Ryu, H. J.; Fortner, D. B.; Lee, S.; Ferebee, R.; De Graef, M.; Misichronis, K.; Avgeropoulos, A.; Bockstaller, M. R. Role of Grain Boundary Defects During Grain Coarsening of Lamellar Block Copolymers. *Macromolecules* **2013**, *46* (1), 204−215.

(16) Ryu, H. J.; Fortner, D. B.; Rohrer, G. S.; Bockstaller, M. R. Measuring Relative Grain-Boundary Energies in Block-Copolymer Microstructures. *Phys. Rev. Lett.* **2012**, *108*, 10.

(17) Campbell, I. P.; He, C. L.; Stoykovich, M. P. Topologically Distinct Lamellar Block Copolymer Morphologies Formed by Solvent and Thermal Annealing. *ACS Macro Lett.* **2013**, *2* (10), 918−923.

(18) Campbell, I. P.; Lau, G. J.; Feaver, J. L.; Stoykovich, M. P. Network Connectivity and Long-Range Continuity of Lamellar Morphologies in Block Copolymer Thin Films. *Macromolecules* **2012**, *45* (3), 1587−1594.

(19) Hashimoto, T.; Nagatoshi, K.; Todo, A.; Hasegawa, H.; Kawai, H. Domain-Boundary Structure of Styrene-Isoprene Block Copolymer Films Cast from Toluene Solutions. *Macromolecules* **1974**, *7* (3), 364−373.

(20) Ryu, H. J.; Bockstaller, M. R. Microstructure evolution in block copolymer blend systems. *Abstr. Pap. Am. Chem. Soc.* **2012**, 243.

(21) Ryu, H. J.; Sun, J.; Avgeropoulos, A.; Bockstaller, M. R. Retardation of Grain Growth and Grain Boundary Pinning in Athermal Block Copolymer Blend Systems. *Macromolecules* **2014**, *47* (4), 1419−1427.

(22) Hu, X. C.; Gido, S. P.; Russell, T. P.; Iatrou, H.; Hadjichristidis, N.; Abuzaina, F. M.; Garetz, B. A. Grain growth kinetics of A(n)B(n) star block copolymers in supercritical. carbon dioxide. *Macromolecules* **2005**, *38* (11), 4719−4728.

(23) Olsen, B. D.; Segalman, R. A. Structure and thermodynamics of weakly segregated rod-coil block copolymers. *Macromolecules* **2005**, *38* (24), 10127−10137.

(24) Born, M.; Wolf, E. *Principles of Optics*, 7th ed.; Cambridge University Press: 1999; pp 837−840.

(25) Garetz, B. A.; Balsara, N. P.; Dai, H. J.; Wang, Z.; Newstein, M. C.; Majumdar, B. Orientation correlations in lamellar block copolymers. *Macromolecules* **1996**, *29* (13), 4675−4679.

(26) Balsara, N. P.; Marques, C. M.; Garetz, B. A.; Newstein, M. C.; Gido, S. P. Anisotropy of lamellar block copolymer grains. *Phys. Rev. E* **2002**, *66* (5), 052802.

(27) Newstein, M. C.; Garetz, B. A.; Balsara, N. P.; Chang, M. Y.; Dai, H. J. Growth of grains and correlated grain clusters in a block copolymer melt. *Macromolecules* **1998**, *31* (1), 64−76.

(28) Dai, H. J.; Balsara, N. P.; Garetz, B. A.; Newstein, M. C. Grain growth and defect annihilation in block copolymers. *Phys. Rev. Lett.* **1996**, *77* (17), 3677−3680.

(29) We have employed two methods for deriving expressions for the depolarized scattered intensity: the correlation function method[25] and the amplitude method.[27] This paper uses the correlation function method. As a result, the parameters l and w in this paper are identical to those in ref 25 but larger than those in ref 27 by a factor of $\sqrt{2}$.

(30) Balsara, N. P.; Garetz, B. A.; Dai, H. J. Relationship between Birefringence and the Structure of Ordered Block Copolymer Materials. *Macromolecules* **1992**, *25* (22), 6072−6074.

(31) Thelen, J. L.; Teran, A. A.; Wang, X.; Garetz, B. A.; Nakamura, I.; Wang, Z. G.; Balsara, N. P. Phase Behavior of a Block Copolymer/Salt Mixture through the Order-to-Disorder Transition. *Macromolecules* **2014**, *47* (8), 2666−2673.

DOI: 10.1021/acs.macromol.7b01048
Macromolecules 2017, 50, 5122−5131

(32) Fasolka, M. J.; Mayes, A. M. Block copolymer thin films: Physics and applications. *Annu. Rev. Mater. Res.* **2001**, *31*, 323−355.
(33) Ilavsky, J. Nika: software for two-dimensional data reduction. *J. Appl. Crystallogr.* **2012**, *45*, 324−328.
(34) Teran, A. A.; Balsara, N. P. Thermodynamics of Block Copolymers with and without Salt. *J. Phys. Chem. B* **2014**, *118* (1), 4−17.
(35) Gavin, H. The Levenberg−Marquardt method for nonlinear least squares curve-fitting problems. Department of Civil and Environmental Engineering, Duke University, 2011.
(36) Abuzaina, F. M.; Garetz, B. A.; Mody, J. U.; Newstein, M. C.; Balsara, N. P. Birefringence and depolarized light scattering from ordered block copolymers with anisotropic distributions of grain orientations produced by shear flow. *Macromolecules* **2004**, *37* (11), 4185−4195.
(37) Chintapalli, M.; Chen, X. C.; Thelen, J. L.; Teran, A. A.; Wang, X.; Garetz, B. A.; Balsara, N. P. Effect of Grain Size on the Ionic Conductivity of a Block Copolymer Electrolyte. *Macromolecules* **2014**, *47* (15), 5424−5431.
(38) Singh, M.; Odusanya, O.; Wilmes, G. M.; Eitouni, H. B.; Gomez, E. D.; Patel, A. J.; Chen, V. L.; Park, M. J.; Fragouli, P.; Iatrou, H.; Hadjichristidis, N.; Cookson, D.; Balsara, N. P. Effect of molecular weight on the mechanical and electrical properties of block copolymer electrolytes. *Macromolecules* **2007**, *40* (13), 4578−4585.
(39) Chintapalli, M.; Higa, K.; Chen, X. C.; Srinivasan, V.; Balsara, N. P. Simulation of local ion transport in lamellar block copolymer electrolytes based on electron micrographs. *J. Polym. Sci., Part B: Polym. Phys.* **2017**, *55* (3), 266−274.
(40) Gunkel, I.; Thurn-Albrecht, T. Thermodynamic and Structural Changes in Ion-Containing Symmetric Diblock Copolymers: A Small-Angle X-ray Scattering Study. *Macromolecules* **2012**, *45* (1), 283−291.
(41) Zardalidis, G.; Gatsouli, K.; Pispas, S.; Mezger, M.; Floudas, G. Ionic Conductivity, Self-Assembly, and Viscoelasticity in Poly(styrene-b-ethylene oxide) Electrolytes Doped with LiTf. *Macromolecules* **2015**, *48* (19), 7164−7171.

DOI: 10.1021/acs.macromol.7b01048
Macromolecules 2017, 50, 5122−5131